Magnetic localization in the spin-polarized one-dimensional Anderson-Hubbard model

M. Okumura,[1,2,*] S. Yamada,[1,2,†] N. Taniguchi,[3,‡] and M. Machida[1,2,§]
[1]*CCSE, Japan Atomic Energy Agency, 6-9-3 Higashi-Ueno, Taito-ku, Tokyo 110-0015, Japan*
[2]*CREST (JST), 4-1-8 Honcho, Kawaguchi, Saitama 332-0012, Japan*
[3]*Institute of Physics, University of Tsukuba, Tennodai, Tsukuba 305-8571, Japan*
(Received 15 April 2009; published 14 May 2009)

In order to study an interplay of disorder, correlation, and spin imbalance on antiferromagnetism, we systematically explore the ground state of one-dimensional spin-imbalanced Anderson-Hubbard model by using the density-matrix renormalization-group method. We find that disorders localize the antiferromagnetic spin-density wave induced by imbalanced fermions and the increase in the disorder magnitude shrinks the areas of the localized antiferromagnetized regions. Moreover, the antiferromagnetism finally disappears above a large disorder. The localization behaviors are observable in atomic Fermi gases loaded on optical lattices as broadening of the momentum distribution of the spin density by using the Stern-Gerlach type of time-of-flight imaging.

DOI: 10.1103/PhysRevB.79.184417 PACS number(s): 71.10.Fd, 03.75.Ss, 71.10.Pm, 71.23.−k

I. INTRODUCTION

An atomic Fermi gas loaded on an optical lattice (FGOL) has been one of the most active target[1,2] since the successful observation of the superfluid-insulator transition in the Bose counterpart.[3] In FGOL, its interaction tunability associated with the Feshbach resonance and lattice formation flexibility due to optical operations offer a great opportunity to systematically study the Hubbard model[4] and its extended versions.[5,6] Thus, FGOL has been regarded as a promising experimental reality to resolve a wide range of controversial issues in condensed-matter physics.[1]

One of main issues in condensed-matter physics is understanding strong electronic correlations. On the other hand, disorder is also of a great importance for transport properties in materials. The Anderson-Hubbard (AH) model has been intensively investigated as a central model to examine both effects.[7–10] However, the interplay between them still remains unsolved.

Recently, the Anderson localization has been directly observed as that of the matter wave in noninteracting cold bosonic gases.[11] Such a direct confirmation is very useful in resolving controversial issues. Thus, we expect that the localization feature in the AH model will be a challenging target[1,5,6] in FGOL. In this paper, we therefore predict the spin-density profile in spin-imbalanced AH model by using the density-matrix renormalization-group (DMRG) method.[12,13]

In FGOL, the spin-imbalance input is tunable and its output effect is also observable.[1,14–16] Moreover, the spin imbalance is expected to bring about a new flavor to localization studies. In fact, the highlight in this paper is that disorders localize antiferromagnetic phases induced by the imbalance and finally eliminate the antiferromagnetism in a strong disorder range. These results are easily detectable through momentum distributions of the spin density obtained by using the Stern-Gerlach type of time-of-flight imaging.[15]

This paper is organized as follows. The model and the numerical method are explained in Sec. II. The numerical results, e.g., the interaction and randomness magnitude dependences of the spin-density profile are presented in Sec. III A. A main finding in Sec. III A is the antiferromagnetic localization with increasing the disorder amplitude. The polarization, system size, and boundary-condition dependencies for the magnetism localization phenomenon are presented in Secs. III B–III D, respectively. In Sec. IV, a way to directly observe the localization behaviors in cold atom experiments is shown. Section V is devoted to the conclusion.

II. MODEL AND METHOD

The Hamiltonian of the one-dimensional AH model is given by

$$H_{\mathrm{AH}} = -t \sum_{\langle i,j\rangle,\sigma} c^{\dagger}_{\sigma i} c_{\sigma j} + \sum_{i,\sigma} \epsilon_i n_{\sigma i} + \sum_{i} U n_{\uparrow i} n_{\downarrow i}, \qquad (1)$$

where $\langle i,j\rangle$ refers to the nearest neighbors i and $j=i\pm 1$, t is the hopping parameter between the nearest-neighbor lattice sites, U is the on-site repulsion, $c_{\sigma i}(c^{\dagger}_{\sigma i})$ is the annihilation (creation) operator and $n_{\sigma i}(\equiv c^{\dagger}_{\sigma i} c_{\sigma i})$ is the site density operator with spin index $\sigma=\uparrow,\downarrow$ and the random on-site potential ϵ_i is chosen by a box probability distribution $\mathcal{P}(\epsilon_i)=\theta(W/2-|\epsilon_i|)/W$, where $\theta(x)$ is the step function and the parameter W the disorder strength magnitude. In DMRG calculations, the number of states kept (m) is 500–700 and these numbers ($m\geq 500$) are enough for the most cases. In the calculations, we apply the open boundary condition except for the comparison with the periodical condition and measure the site matter and spin density of fermions as $n_{\uparrow i}\pm n_{\downarrow i}$.

III. MAGNETISM LOCALIZATION

A. Interaction and randomness dependences

Let us show DMRG calculation results on spin-imbalanced AH model (1). Figure 1 displays a randomness amplitude (W/t) dependence of the on-site matter and spin-density profile for the number of the total sites $L=100$ the number of the spin-up and spin-down fermions $(N_{\uparrow},N_{\downarrow})=(51,49)$ (half filling) and $U/t=10$. In this case, two up-spin

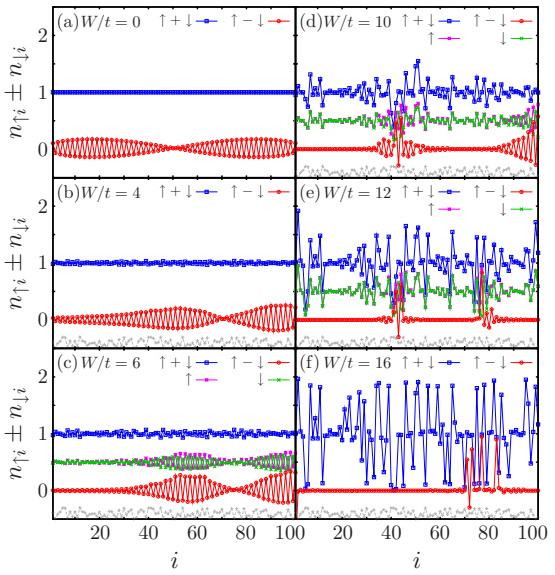

FIG. 1. (Color online) The randomness magnitude W dependence of the matter and spin-density profiles ($n_{\uparrow i} \pm n_{\downarrow i}$, respectively) at the half filling for $U/t=10$ with $(N_\uparrow, N_\downarrow)=(51,49)$. A profile of the selected random potential is depicted on the bottom of each figure in an arbitrary unit (gray dashed line). In (c)–(e), up- and down-spin-density profiles are shown. For all calculations, m is 500.

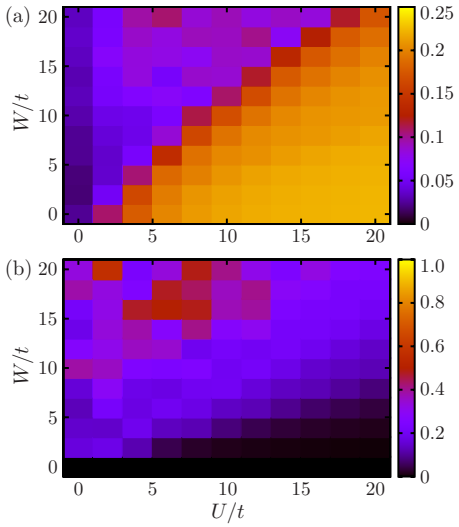

FIG. 2. (Color online) Contour plots of the value of (a) $S(U,W)$ [Eq. (2)] and (b) $D(U,W)$ [Eq. (3)] with $L=100$ and $(N_\uparrow, N_\downarrow)=(101,99)$ at the half filling in a range of U $(0 \le U \le 20)$ and W $(0 \le W \le 20)$. The step value for both U/t and W/t is 2. For all calculations, m is 500.

fermions do not have their (down-spin) partners. The matter density profile is almost flat for $W \le U$ as seen in Figs. 1(a)–1(c) while it is drastically disturbed for $W \ge U$. This is completely the same as that of the balanced case. However, the spin-density profile is significantly different. First, in the clean case as shown in Fig. 1(a) $(W/t=0)$ one finds an antiferromagnetic spin-density wave (ASDW) whose periodicity is found to be inversely proportional to $N_\uparrow - N_\downarrow$ [e.g., see Figs. 3(h) and 3(i) in which $N_\uparrow - N_\downarrow = 2$ and 4, respectively]. Here, it is noted that any ASDW phases are never observed in the perfectly balanced cases irrespective of the presence of randomness.[17] This clearly indicates that the imbalance is responsible for the ASDW phase. Second, as one increases the disorder strength a part of the ASDW (amplitude) "locally" vanishes and the depressed regions expand as seen in Figs. 1(b) and 1(c). This tendency becomes remarkable when W exceeds U as seen in Figs. 1(d) and 1(e) in which two ASDW phases are localized and isolated from each other. This isolation can be explained by the complete localization of two excess up-spin fermions for $W > U$ since the ASDW can be created only at the localized spots of the excess up-spin particles. The further increase in W diminishes the antiferromagnetic structure as seen in Fig. 1(f) in which the localized structure is characterized by positive peaks instead of the staggered (plus-minus) moment alternation. This is because the strong randomness fully dominates over the other effects. However, we note here that it is difficult in this large disorder range to judge whether the result [Fig. 1(f)] is the true ground state or not. The reason is that in this strong W range tiny changes in W (e.g., $W+\delta W$) give entirely different spin-density distributions in noncontinuous manner which is not observed when $0 < W/t \le 14$. Generally, it is well known in strongly glassy situations that a tiny change in calculation parameters results in a drastic different consequence. Thus, we expect that there are a lot of local minima in this strong disorder range. Figure 1(f) is a localization profile selected among those minima.

In order to characterize the spin-density profile in a wide range of U and W we define the following function:

$$S(U,W) = \left\langle \sum_{i=1}^{L} \frac{|n_{\uparrow i}(\epsilon,U,W) - n_{\downarrow i}(\epsilon,U,W)|}{L} \right\rangle_\epsilon, \qquad (2)$$

where $n_{\sigma i}(\epsilon,U,W)$ is the local site density under a random potential symbolically specified by ϵ at a certain set of U and W, and $\langle \cdot \rangle_\epsilon$ means an algebraic average for various random realizations. From the expression, it is found that $S(U,W)$ gives an indicator how large the spin moment develops on each site. If the staggered moment widely grows then $S(U,W)$ gives a relatively large value. Thus, a map of $S(U,W)$ in a wide range of U and W is expected to clarify an interplay of U and W on the ASDW phase localization. Figure 2(a) shows a contour plot of $S(U,W)$, which is averaged over ten realizations of random potentials for $L=100$ and $(N_\uparrow, N_\downarrow)=(51,49)$. In this figure, when one increases W along a fixed U/t line (e.g., $U/t=10$ line) from $W/t=0$ to 20, it is found that the averaged moment of ASDW very slowly decreases inside the region $W < U$. This is consistent with the spin-density profile as seen in Figs. 1(a)–1(c) in which the areas of ASDW phases slowly diminish with increasing W. When W exceeds U, the variation in $S(U,W)$ suddenly changes to a fast suppression. This reflects the change in the localization of the excess up-spin particles as seen in Figs. 1(c) and 1(d).

In order to qualify the present randomness averaging in Fig. 2(a) we introduce the following function:

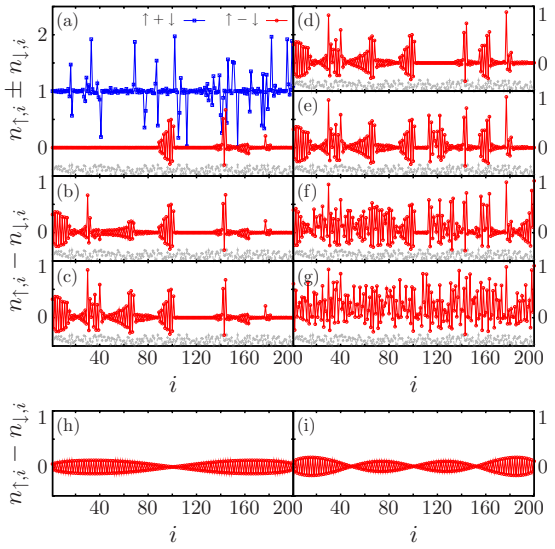

FIG. 3. (Color online) The polarization dependence of the spin-density profiles [(a)–(g)] with $U/t=W/t=20$ and that without random potential [(h) and (i)] at $U/t=20$. The last two figures, (h) and (i), without the randomness are displayed for a comparison with disordered cases (a) and (b), respectively. The number of up- and down-spin particles $(N_\uparrow,N_\downarrow)$ are (a) (101,99), (b) (102,98), (c) (103,97), (d) (104,96), (e) (105,95), (f) (110,90), (g) (120,80), (h) (101,99), and (i) (102,98), respectively. The random potential shapes are displayed on the bottom of (a)–(g) (gray dashed lines). For all calculations, m is 600.

$$D(U,W) = \sqrt{\left\langle \left[\frac{S_\epsilon(U,W)}{S(U,W)} - 1 \right]^2 \right\rangle_\epsilon}. \quad (3)$$

This corresponds to a standard deviation on the randomness average. Figure 2(b) is a contour map of $D(U,W)$ in the same range as Fig. 2(a). One finds that in a small W/t range $D(U,W)$ shows a very small value (almost zero) and $D(U,W)$ reaches about 0.2 around $W=U+3t\sim4t$ line when increasing W/t at a constant U/t. Thus, the averaged values in Fig. 2(a) are sufficiently qualified except for above $W=U+3t$ line. This result means that the qualitative change as observed around $W=U$ in Fig. 2(a) is not a side effect associated with the averaging but an essential feature in this system.

B. Polarization dependence

Next, we investigate the polarization strength dependence of the spin-density profile.[18] Figures 3(a)–3(g) display the correspondent results made at the half filling in $L=200$, $U/t=18$, and $W/t=20$. In the range of these parameters, clear localization of the ASDW phases can be observed with the phase separation from the nonmagnetized phases. First, Fig. 3(a) displays the charge and spin-density distributions in $(N_\uparrow,N_\downarrow)=(101,99)$. One finds two magnetized regions in which ASDW phases are localized with the localization of two extra fermions. The slight increase in the polarization $[(N_\uparrow,N_\downarrow)=(102,98)]$ increases the number of the magnetized regions as seen in Fig. 3(b). Here, we note that the magnetized places formed in the less polarized case as Fig. 3(a) are still kept. This is in contrast to the clean systems $(W/t=0)$ as shown in Figs. 3(h) and 3(i) whose polarizations are the same as Figs. 3(a) and 3(b), respectively. This is a typical feature characteristic to disordered systems in which memory effects can be frequently observed. The further increase in the polarization extends the magnetized regions as shown in Figs. 3(c)–3(g). In Fig. 3(g), the magnetized (ASDW) regions cover all sites, which are almost positively polarized although the alternation profile still remains.

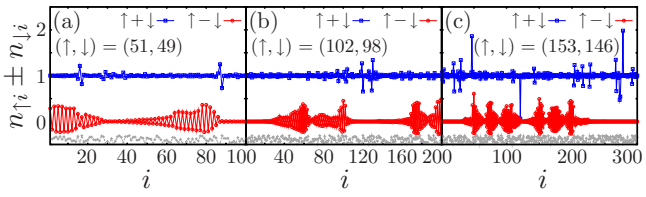

FIG. 4. (Color online) The size dependence of the matter and spin-density profiles. The same polarization ratio is kept. (a) $L=100$ case with $(N_\uparrow,N_\downarrow)=(51,49)$, (b) $L=200$ case with $(N_\uparrow,N_\downarrow)=(102,98)$, and (c) $L=300$ case with $(N_\uparrow,N_\downarrow)=(153,147)$, respectively. $U/t=W/t=20$ in all cases. The random potential profiles are shown on the bottom of each figure (gray dashed lines). For all calculations, m is 600.

C. System size dependence

Now, let us check a system size dependence of this magnetism localization to confirm that it is not a small size effect. In Figs. 4(a)–4(c), we show the charge and spin-density distributions at $U/t=W/t=20$ in $L=100$, 200, and 300 with $(N_\uparrow,N_\downarrow)=(51,49)$, (102,98), and (153,147), respectively. We clearly find that these all cases exhibit the same qualitative behavior, i.e., the magnetized regions are localized with the separation from the nonmagnetized regions. From these figures we find that the observed magnetism localization is an intrinsic effect.

D. Boundary condition dependence

Let us re-examine model (1) under the periodic boundary condition to check the effect of the boundary condition. Figures 5(a)–5(f) show the W-dependent charge and spin-density profiles in the periodic condition. In Fig. 5(a) $(W/t=0)$, we find complete flat distributions in both the charge and spin densities. They are characteristic to the periodic boundary condition in which the excess fermions fully distribute homogeneously. This is in contrast to the open boundary condition [compare it with Fig. 1(a)]. When the randomness is added into the system the ASDW phases are induced as seen in Figs. 5(b) and 5(c). Thus, one finds that the ASDW phase requires two conditions, i.e., the imbalance and the translational symmetry breaking. When the randomness strength increases one finds that the amplitude of the ASDW increases [see Figs. 5(b) and 5(c)]. This implies that the localization of extra two fermions proceeds with increasing W/t. At $W/t=12$ and 14 [see Figs. 5(d) and 5(e) for $W>U$], we find the phase separation from the nonmagnetized phases, which is the same as the open boundary case. Further increase in W/t brings about more tight localization [Fig. 5(e)]

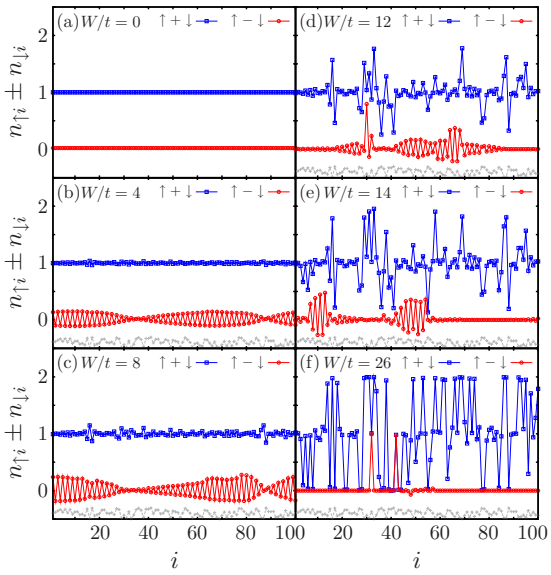

FIG. 5. (Color online) The randomness W-dependent matter and spin-density profiles ($n_{\uparrow i}\pm n_{\downarrow i}$, respectively) with $L=100$, $(N_\uparrow,N_\downarrow)=(51,49)$, and $U/t=10$, under a random potential depicted on the bottom of each figure in arbitrary unit (gray dashed line). The periodic boundary condition is employed. For all calculations, m is 700.

and disappearance of the staggered moment profile [Fig. 5(f)]. This is also the same as the open boundary case.

IV. EXPERIMENTAL DETECTION

Finally, we discuss how to detect this phenomenon in FGOL. Our idea is to measure spin-dependent momentum distributions because localization in positional space gives broadening in momentum space due to the uncertainty principle in quantum mechanics. In cold atom experiments, the Stern-Gerlach type of time-of-flight imaging (ToFI) can watch momentum distributions of different spin species separately at a time.[15] In Fig. 6, we show quasimomentum distributions of the spin density $n_{\uparrow k}-n_{\downarrow k}$, where $n_{\sigma k}=\langle c^\dagger_{\sigma k}c_{\sigma k}\rangle$, $c_{\sigma k}=[2/(L+1)]^{1/2}\Sigma_{i=1}^{L}\sin(ki)c_{\sigma i}$, and k is the quasimomentum defined as $k=n\pi/(L+1)$ $(n=1,2,\ldots,L)$.[19] One finds a single peak structure in the $W/t=0$ case in which the ASDW uniformly extends [see Fig. 1(a)] while one identifies

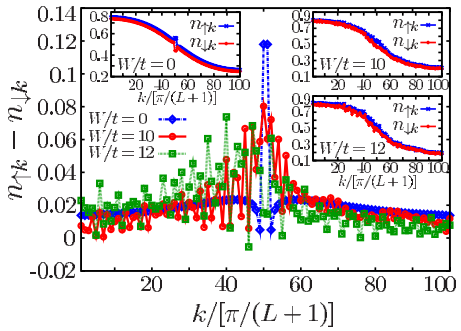

FIG. 6. (Color online) The quasimomentum distributions of spin density $n_{\uparrow k}-n_{\downarrow k}$ for Fig. 1(a) $(W/t=0)$, Fig. 1(d) $(W/t=10)$, and Fig. 1(e) $(W/t=12)$. The insets show quasimomentum distributions for different spins ($n_{\uparrow k}$ and $n_{\downarrow k}$, respectively) in each case.

broadened momentum distributions in the $W/t=10$ and 12 cases, which exhibit the magnetism localization [see Figs. 1(d) and 1(e)]. In both the latter cases we note that the peak structure still remains. This arises from the ASDW still lying inside the localized clusters [Figs. 1(d) and 1(e)].

V. CONCLUSION

In conclusion, we systematically studied the polarized AH model at the half filling and found that the disorder localizes the ASDW phases induced by the excess fermions. As the randomness strength increases the areas of the localized ASDW phases shrink with the expansion of the nonmagnetized areas and the antiferromagnetism finally vanishes. Moreover, we proposed in FGOLs that ToFI technique can identify the magnetism localization. The observed spin-density quasimomentum distribution exhibits significant broadening when the magnetism localization occurs.

ACKNOWLEDGMENTS

The authors wish to thank H. Aoki, T. Deguchi, K. Iida, T. Koyama, H. Matusmoto, Y. Ohashi, T. Oka, S. Tsuchiya, and Y. Yanase for illuminating discussion. The work was partially supported by Grant-in-Aid for Scientific Research under Grant No. 20500044 and one on Priority Area "Physics of new quantum phases in superclean materials" under Grant No. 20029019 from MEXT, Japan. One of authors (M.M.) is supported by JSPS Core-to-Core Program-Strategic Research Networks, "Nanoscience and Engineering in Superconductivity."

*okumura.masahiko@jaea.go.jp
†yamada.susumu@jaea.go.jp
‡taniguch@sakura.cc.tsukuba.ac.jp
§machida.masahiko@jaea.go.jp

[1] For recent reviews, see, e.g., M. Lewenstein, A. Sanpera, V. Ahufinger, B. Damski, A. Sen, and U. Sen, Adv. Phys. **56**, 243 (2007); I. Bloch, J. Dalibard, and W. Zwerger, Rev. Mod. Phys. **80**, 885 (2008), and references therein.

[2] For the latest advancement, see, e.g., R. Jördens, N. Strohmaier, K. Günter, H. Moritz, T. Esslinger, Nature (London) **455**, 204 (2008); U. Schneider, L. Hackermüller, S. Will, Th. Best, I. Bloch, T. A. Costi, R. W. Helmes, D. Rasch, and A. Rosch, Science **322**, 1520 (2008).

[3] M. Greiner, O. Mandel, T. Esslinger, T. W. Hänsch, and I. Bloch, Nature (London) **415**, 39 (2002).

[4] M. Machida, M. Okumura, and S. Yamada, Phys. Rev. A **77**, 033619 (2008).

[5] X. Gao, M. Polini, B. Tanatar, and M. P. Tosi, Phys. Rev. B **73**, 161103(R) (2006); X. Gao, *ibid.* **78**, 085108 (2008); **78**, 249901 (2008).

[6] M. Okumura, S. Yamada, N. Taniguchi, and M. Machida, Phys. Rev. Lett. **101**, 016407 (2008).
[7] P. W. Anderson, Phys. Rev. **109**, 1492 (1958).
[8] J. Hubbard, Proc. R. Soc. London, Ser. A **240**, 539 (1957); **243**, 336 (1958).
[9] M. Ma, Phys. Rev. B **26**, 5097 (1982); A. W. Sandvik, D. J. Scalapino, and P. Henelius, *ibid.* **50**, 10474 (1994); Y. Otsuka, Y. Morita, and Y. Hatsugai, *ibid.* **58**, 15314 (1998); R. V. Pai, A. Punnoose, and R. A. Römer, arXiv:cond-mat/9704027 (unpublished).
[10] Another context is the persistent current in mesoscopic rings, which is not cited in this paper. For its recent progress, see, e.g., E. Gambetti, Phys. Rev. B **72**, 165338 (2005), and references therein.
[11] J. Billy, V. Josse, Z. Zuo, A. Bernard, B. Hambrecht, P. Lugan, D. Clément, L. Sanchez-Palencia, P. Bouyer, and A. Aspect, Nature (London) **453**, 891 (2008); G. Roati, C. D'Errico, L. Fallani, M. Fattori, C. Fort, M. Zaccanti, G. Modugno, M. Modugno, and M. Inguscio, *ibid.* **453**, 895 (2008); J. Chabé, G. Lemarié, B. Grémaud, D. Delande, P. Szriftgiser, and J. C. Garreau, Phys. Rev. Lett. **101**, 255702 (2008).
[12] S. R. White, Phys. Rev. Lett. **69**, 2863 (1992); Phys. Rev. B **48**, 10345 (1993).
[13] For recent reviews, see, e.g., U. Schollwöck, Rev. Mod. Phys. **77**, 259 (2005); K. A. Hallberg, Adv. Phys. **55**, 477 (2006), and references therein.
[14] M. W. Zwierlein, A. Schirotzek, C. H. Schunck, and W. Ketterle, Science **311**, 492 (2006); G. B. Partridge, W. Li, R. I. Kamar, Y. A. Liao, and R. G. Hulet, *ibid.* **311**, 503 (2006); M. W. Zwierlein, A. Schirotzek, C. H. Schunck, and W. Ketterle, Nature (London) **442**, 54 (2006); Y. Shin, M. W. Zwierlein, C. H. Schunck, A. Schirotzek, and W. Ketterle, Phys. Rev. Lett. **97**, 030401 (2006); G. B. Partridge, W. Li, Y. A. Liao, R. G. Hulet, M. Haque, and H. T. C. Stoof, *ibid.* **97**, 190407 (2006); C. H. Schunck, Y. Shin, A. Schirotzek, M. W. Zwierlein, and W. Ketterle, Science **316**, 867 (2007).
[15] J. Stenger, S. Inouye, D. M. Stamper-Kurn, H.-J. Miesner, A. P. Chikkatur, and W. Ketterle, Nature (London) **396**, 345 (1998).
[16] M. Machida, M. Okumura, S. Yamada, T. Deguchi, Y. Ohashi, and H. Matsumoto, Phys. Rev. B **78**, 235117 (2008).
[17] In this system, $N_\uparrow$ and $N_\downarrow$ are noted to be conserved, respectively. They are also essentially conserved in FGOL.
[18] We confirmed no qualitative difference between several different realizations of random potentials. Therefore, we show typical examples in Fig. 3.
[19] E. Jeckelmann, Prog. Theor. Phys. Suppl. **176**, 143 (2008).